NASA TECHNICAL NOTE

NASA TN D-5851

C. 1

NASA TN D-5851

PHENOMENOLOGICAL AND STATISTICAL ANALYSIS OF FRACTURE IN POLYCRYSTALLINE ALUMINUM OXIDE

by Thomas M. Heslin and Alfred G. Eubanks

Goddard Space Flight Center
Greenbelt, Md. 20771

NATIONAL AERONAUTICS AND SPACE ADMINISTRATION • WASHINGTON, D. C. • AUGUST 1970

1. Report No. NASA TN D-5851	2. Government Accession No.	3. Recipient's Catalog No.
4. Title and Subtitle Phenomenological and Statistical Analysis of Fracture in Polycrystalline Aluminum Oxide		5. Report Date August 1970
		6. Performing Organization Code
7. Author(s) Thomas M. Heslin and Alfred G. Eubanks		8. Performing Organization Report No. G-984
9. Performing Organization Name and Address Goddard Space Flight Center Greenbelt, Maryland 20771		10. Work Unit No. 601-13-02-42-51
		11. Contract or Grant No.
		13. Type of Report and Period Covered Technical Note
12. Sponsoring Agency Name and Address National Aeronautics and Space Administration Washington, D. C. 20546		14. Sponsoring Agency Code
15. Supplementary Notes		

16. Abstract

Flaws in 20 polycrystalline aluminum oxide flexure specimens were studied. Using the maximum linear dimension of pores and grain pullouts, an exponential distribution was fitted to an observed cumulative flaw "magnitude" distribution, and its associated largest value distribution calculated. A comparison of these calculated values with actual values from gauge-size pieces of failed samples was made, and a comparison of results therefrom with the Griffith equation showed that the latter describes the data reasonably well.

17. Key Words Suggested by Author: Aluminum oxide flaws; Ceramic materials flaws; Flaws in aluminum oxide; Flaws in ceramic materials		18. Distribution Statement: Unclassified - Unlimited	
19. Security Classif. (of this report) Unclassified	20. Security Classif. (of this page) Unclassified	21. No. of Pages 20	22. Price* $3.00

*For sale by the Clearinghouse for Federal Scientific and Technical Information
Springfield, Virginia 22151

SUMMARY

A correlation procedure which relates strength to flaw "magnitude" is reviewed and presented for ceramic materials. The procedure was applied to 20 nominally identical polished polycrystalline aluminum-oxide flexure specimens. Using the maximum linear dimension of pores and grain pull-outs in the flexure specimens as a measure of the stress-concentrating ability of surface flaws, an exponential distribution was fitted to an observed cumulative flaw "magnitude" distribution, and its associated largest value distribution calculated. These calculated values were compared with values which were observed on gauge-size pieces of failed samples. Using this largest value distribution, flaw magnitude and strength were correlated and the results compared with the Griffith equation. The comparison showed that equations with the Griffith form describe the data reasonably well. The comparison served to define clearly the correlation procedure and problems that are associated with its application.

CONTENTS

PHENOMENOLOGICAL AND STATISTICAL ANALYSIS OF FRACTURE IN POLYCRYSTALLINE ALUMINUM OXIDE

by
Thomas M. Heslin and Alfred G. Eubanks
Goddard Space Flight Center

INTRODUCTION

According to the "weakest-link" model, a material has a unique strength called its "theoretical strength," which is of the order of 10^6 psi for ceramics. This strength does not in general actually exist, because of the presence of numerous flaws, each of which acts as a stress concentrator. Fracture occurs when the peak stress adjacent to the single, most acute flaw in a body reaches the "theoretical strength" of the material. Of course, this strength is purely conceptual in nature, as one cannot test the strength of an isolated element without changing the conditions that exist when the element is actually in the body. In addition to this indeterminacy, there is an uncertainty associated with the statistical nature of the concept itself which is considered by some investigators to be an inherent property of materials. This inherent uncertainty arises because the acuteness of the most severe flaw in a specimen may differ for individual specimens in a nominally identical set. Thus, if flaw "magnitudes" are statistically distributed in the parent body from which a set of test samples is taken, there is a second statistical distribution, related to the first, for the most severe flaw which exists in samples taken from the parent (Reference 1). It is generally assumed that this distribution is directly related to an observable relationship commonly referred to as the fracture probability. The fracture probability, denoted $S(\sigma)$, is defined (Reference 2) by

$$S(\sigma) = \frac{m}{N+1}, \tag{1}$$

where N is the total number of samples tested; m is the specimen serial number corresponding to a list of fracture stresses arranged in an increasing order from 1 to N; σ is the observed fracture stress for a given m.

The mathematics involved in the weakest-link model is identical to the sampling problem in statistics of finding the least value in samples of size n, drawn from a population with a known value distribution (Reference 3).

If the stress-concentrating ability, or "magnitude," of a flaw is denoted by "c", and strength is assumed to be an inverse function of c, then strength and flaw "magnitude" can be related by finding a cumulative distribution, $F(1/c)$, for the flaw population in the parent body. Given $F(1/c)$, a cumulative distribution of the smallest value, $G(1/c)$, in samples of size n is given (Reference 3) by

$$G\left(\frac{1}{c}\right) = 1 - \left[1 - F\left(\frac{1}{c}\right)\right]^n . \quad (2)$$

It is assumed that this distribution is directly related to the observed fracture probability, $S(\sigma)$, and that strength and flaw "magnitude" can be correlated by comparing $1/c$ and σ for equal values of $G(1/c)$ and $S(\sigma)$.

The study objectives were to establish the types of surface flaws present in a polycrystalline aluminum oxide compact by thoroughly characterizing samples and to define more clearly the procedure outlined and the problems associated with its application.

CHARACTERIZATION AND TESTING

Twenty 5" by 1/2" by 1/8" flexure specimens of 99.5 percent Al_2O_3 were procured. A tabulation of various characterization parameters is given in Table 1. The 5" by 1/2" surfaces of the

Table 1

Quantitative Characterization of Flexure Specimens.

Specimen Serial Number	Modulus of Rupture $\times 10^{-3}$ (psi)	Porosity (%)	Average Grain Size (μ)	Average Linear Flaw Density (counts/inch)	Average (CLA) (micro-inches)	Average Areal Flaw Density $\times 10^{-5}$ (counts/sq. in.)	Largest Flaw $\times 10^3$ (inches)
1	26.959	4.378	24.43	256	4.27	9.54	4.43
2	27.807	4.128	23.67	392	6.69	12.9	5.00
3	27.952	4.413	23.67	357	7.11	10.3	6.25
4	29.022	3.840	16.11	251	3.17	10.4	5.92
5	29.563	5.477	17.85	388	4.87	11.0	5.06
6	29.720	4.242	25.53	237	3.41	10.9	5.16
7	30.012	4.245	20.32	194	3.91	8.11	5.58
8	30.452	4.213	26.56	252	4.21	9.05	5.21
9	31.078	4.249	24.61	299	5.31	6.46	6.00
10	31.168	4.149	17.80	281	5.20	5.78	4.95
11	31.315	4.357	13.13	287	5.00	7.12	5.93
12	31.908	4.038	23.02	408	5.18	18.8	5.81
13	32.937	4.459	26.87	240	4.26	9.09	5.16
14	34.675	5.037	11.05	439	5.19	11.1	5.09
15	34.721	5.223	11.03	397	3.78	11.1	5.46
16	34.846	5.536	11.73	448	4.29	12.6	4.62
17	34.914	5.011	11.99	362	4.72	10.7	5.10
18	34.948	5.528	14.96	455	4.20	13.8	5.17
19	36.181	4.348	15.60	221	3.06	6.89	5.77
20	36.314	5.571	12.34	381	4.31	12.8	4.86

samples were polished by the vendor and had surface roughnesses ranging from 3.06 microinches to 7.11 microinches CLA (center line average). Photomicrographs of a sample, as received and after thermal etching, are shown in Figure 1. The samples were failed in the four-point flexure fixture shown in Figure 2. This fixture is designed to meet the specifications of ASTM method C78-64. The gauge region is 1-1/3" long. The fixture is activated by placing it in the compression stroke of an Instron Model TTC testing machine. The top and bottom of the fixture are attached magnetically to the Instron machine's traveling head and compression cell, respectively. The side posts serve only to initially align the fixture, and are dropped free of the action before testing.

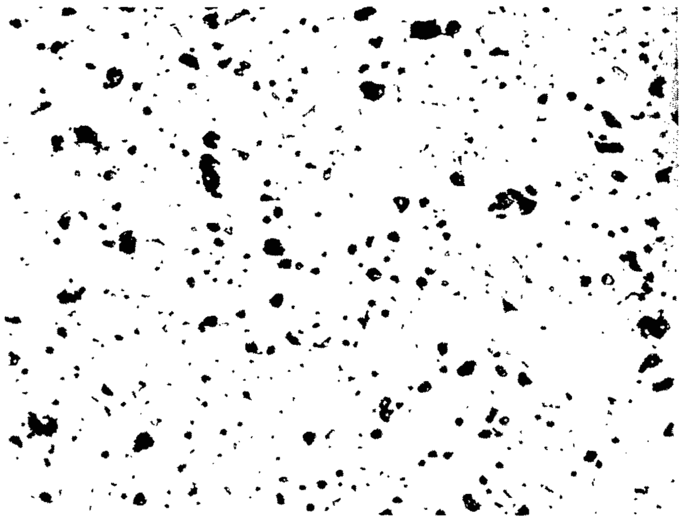

Before thermal etching
215x

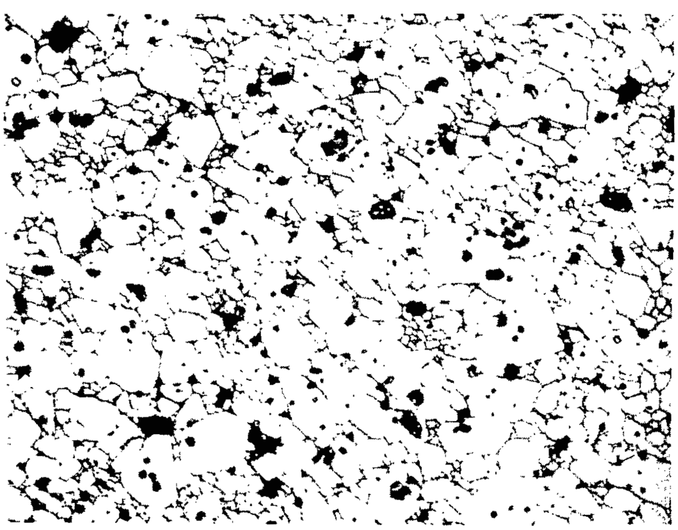

After thermal etching
215x

Figure 1—Sample 15 before and after thermal etching.

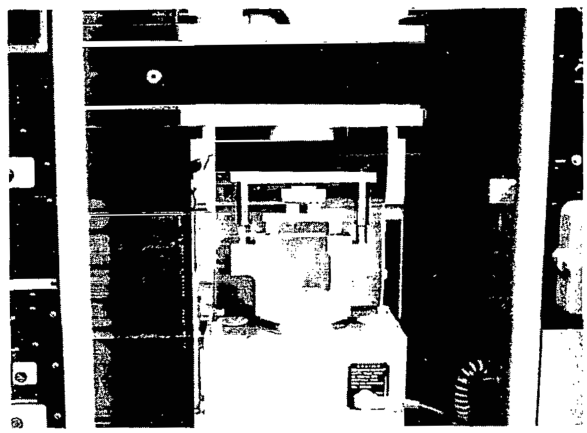

Figure 2—Failure fixture.

A spectrochemical analysis for magnesium and chromium additives of the as-received material was performed and showed chromium and magnesium present in average amounts of 0.23 wt percent and 0.17 wt percent, respectively. Bulk porosities of the samples were determined by comparison of measured density to the theoretical density of 3.987g./cc. The porosity ranged from a high of 5.571 percent to a low of 3.840 percent. Grain size was measured by thermally etching pieces of failed specimens, photographing them, and measuring the intercepts of 120 grains with lines drawn across the photomicrograph. Grain size ranged from a maximum of 26.87 microns to a minimum of

11.03 microns. Areal flaw density was measured by counting the number of pores and grain pull-outs in two 215× photomicrographs of each specimen. One of the photographs was taken near the center of the gauge area; the other was taken near the long edge of the gauge area on the tension surface. The flaw densities ranged from a maximum of 1.88×10^6 flaws/in.^{2} to a minimum of 5.78×10^5 flaws/in.^{2} Linear flaw density was measured by means of a Talysurf 4 profilometer and by counting the spike-like depressions in two profiles, each of which had 10,000× vertical magnification, 500× horizontal magnification, and a 0.3-inch stylus traverse. A representative profile example is shown in Figure 3. One profile was taken near the center of the gauge area, while the other was taken near the long edge of the area. Linear flaw density ranged from a maximum of 455 flaws/in. to a minimum of 221 flaws/in.

A piece of a failed specimen was submitted to X-ray analysis to determine whether there was any preferred orientation of surface crystallites. None was found. Fracture surfaces and areas adjacent to fracture surfaces were examined with a scanning electron microscope (SEM); representative pictures are shown in Figures 4 and 5. Replicas were made of fracture surfaces and examined with a transmission electron microscope. Representative photographs of the surface using this technique are shown in Figure 6. Some samples had hairline cracks branching off from the main fracture. One such crack was examined before and after thermal etching, and is shown in Figure 7. Another such crack was examined with the scanning electron microscope before and after thermal etching; it is shown in Figure 8. Pits at points of dislocation termination were observed on individual grains after thermal etching. An example of this type of flaw is shown in

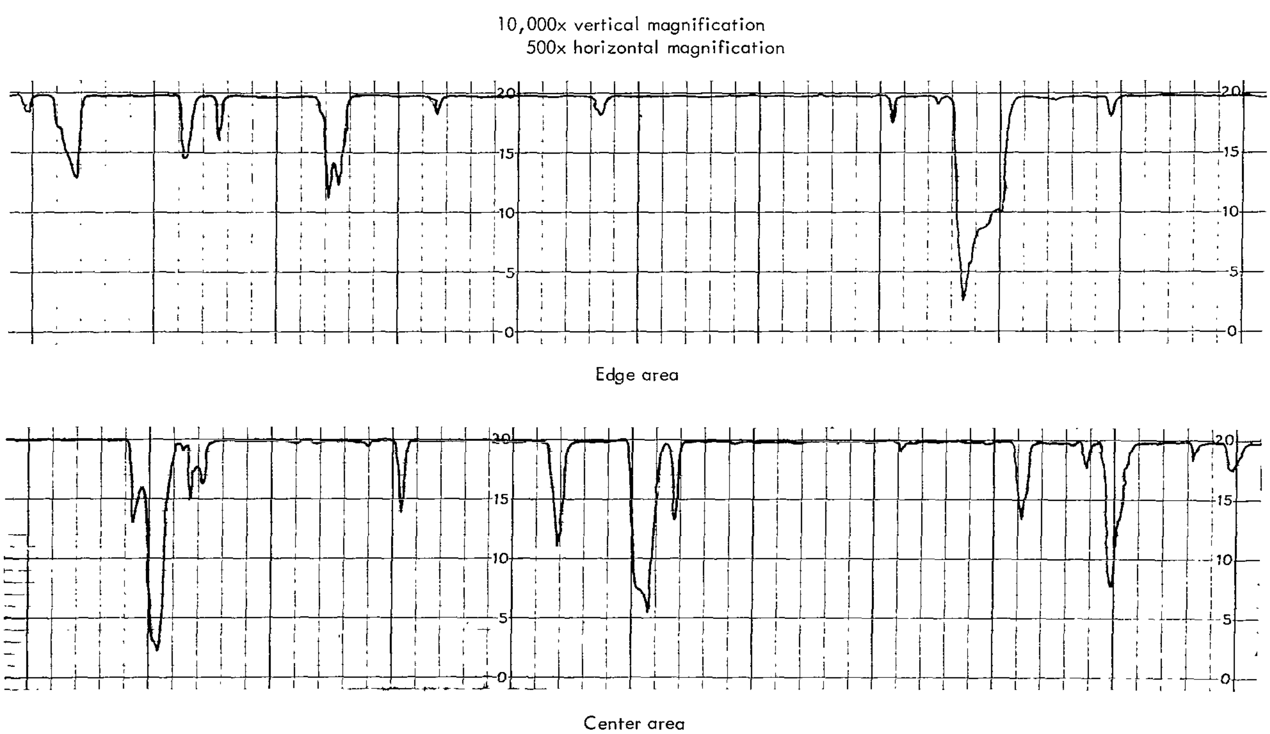

Figure 3—Profiles of sample 9.

Edge area near compression surface
630x

Edge area near tension surface
590x

Center area
730x

Figure 4—Fracture surface viewed through SEM.

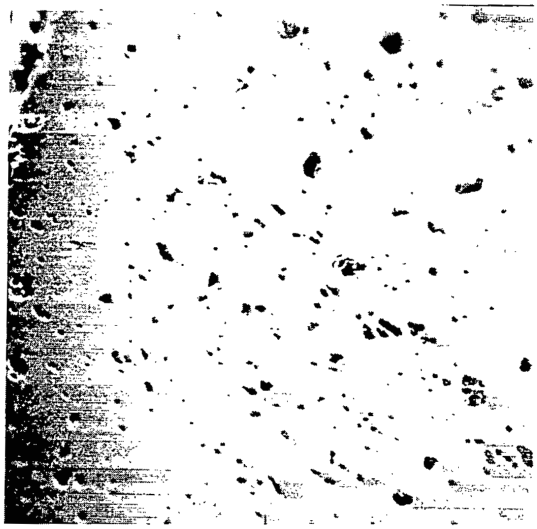

195x

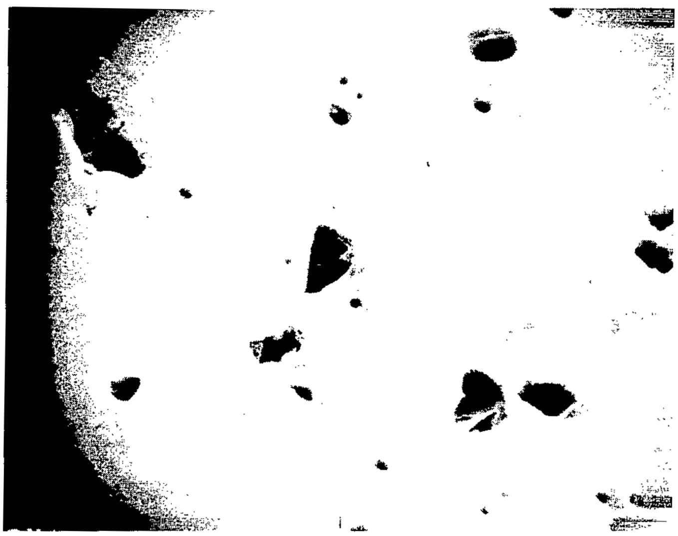

980x

Figure 5—Unetched material viewed through SEM.

2500x

2500x

2500x

Figure 6—Fracture surface viewed through transmission electron microscope.

Before thermal etching
195x

Before thermal etching
900x

After thermal etching
195x

Figure 7—Hairline crack before and after thermal etching.

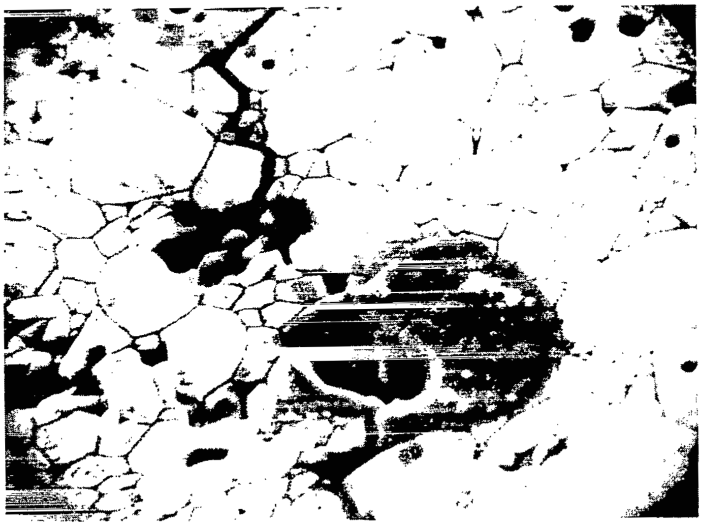

After thermal etching
900x

Figure 8—Hairline crack before and after thermal etching viewed through SEM.

Figure 9. The square geometry of some of the pits indicates that magnesium is present as magnesia and that there are grains of the magnesia dispersed in the body.

The above characterization techniques revealed the presence of five types of flaws in these bodies. They are: pores; grain pullouts from polishing; polishing scratches; grain boundaries;

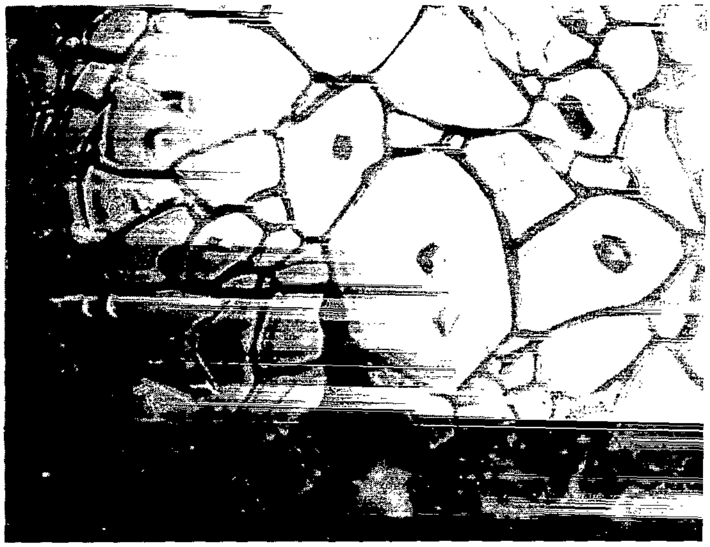

1000x

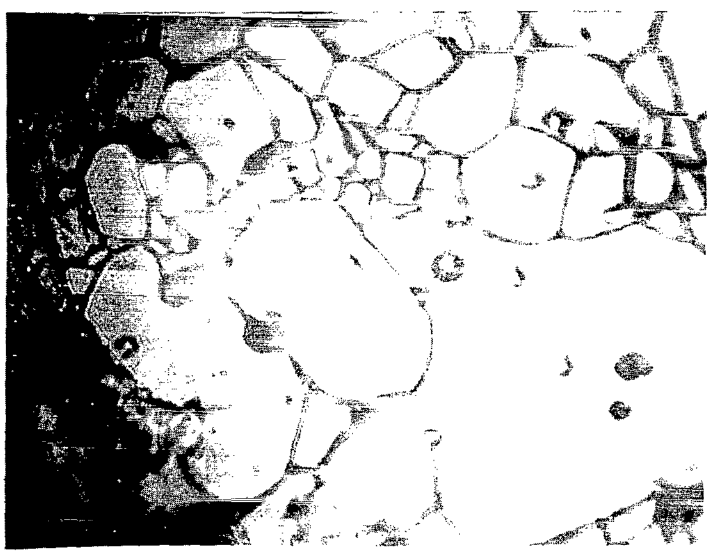

1000x

Figure 9—Pictures showing etch pit in individual grains.

and dislocations in individual grains. Twin boundaries in individual grains have been reported by some investigators (Reference 4); however, any irregularities that could have been attributed to a twin boundary were not observed in these samples. The interaction of the flaw networks present precludes separation of types and prevents superposition of their effects, and thus makes precise determination of the nucleating flaw an extremely difficult task. The most pronounced flaws observed on the polished surface of the samples were holes due to pores and grain pullouts. The fracture path in failed specimens seemed to include as many of these holes as possible.

Grain boundaries also are a pronounced feature, but only after the polished damage layer has been removed by thermal etching. The damage layer probably has tensile properties that are quite different from the bulk material; and it is difficult to determine whether fracture actually nucleates in this layer, or just below it at the interface of the grain boundary and the damage layer.

Grain boundaries are a prime candidate for consideration as fracture-nucleating flaws. It has been fairly well established that thermal expansion and elastic anisotropy at grain boundaries are major causes of weakness in macroscopic bicrystals (References 5 and 6). However, on the microscopic scale of a polycrystalline compact, the forces across the curved peripheral boundaries between particles, which drive the sintering process and tend to pull the grains together, would be of great significance; but such forces would be relatively unimportant for a macroscopic bicrystal. The cohesive force system between particles in the two instances is somewhat different. There is thus some uncertainty in directly extrapolating results obtained with macroscopic samples to a microscopic situation.

It was impossible to firmly classify fracture of these 20 samples as occurring between or across grains, because instances of both types of propagation were observed. Considering these facts, and for lack of a more prominent irregularity on unetched, polished surfaces, it was assumed that pores and grain pullouts were fracture-nucleating flaws. The most obvious and easily made measurement of pores and grain pullouts is their maximum linear dimension as measured from photomicrographs. It was assumed that this dimension is an indication of the stress-concentrating ability of pores and grain pullouts.

The flaw measurement procedure was as follows. Two 215× photomicrographs were taken in the gauge area of each of the 20 samples. A grid was then put over the pictures, and the maximum linear dimension of each pore and grain pullout was measured using a pair of dial calipers. These measurements ranged from 0.01 to 0.85 inches. The measurements were arranged in increasing order; and the number of flaws, n, in each 0.010 inch interval was taken as the number of flaws with magnitude equal to the center value of that particular interval. Flaw magnitude values, denoted c, were calculated, and values of $1/c$ tabulated along with the cumulative number, Σn, of flaws with value less than $1/c$. This information is shown in Table 2. A cumulative flaw distribution was found by dividing values of Σn by the total number of flaws, N, counted in all the photographs. This cumulative flaw distribution was taken as representing the parent flaw distribution, $F(1/c)$.

Table 2

Tabulation for a Cumulative Flaw Distribution for 20 Specimens.

Interval Center (in.)	$c \times 10^4$ (in.)	$\frac{1}{c} \times 10^{-2}$ (in.$^{-1}$)	n	Σn	$\frac{\Sigma n}{N}$	$\log\left(1 - \frac{\Sigma n}{N}\right)^{-1}$
0.015	0.698	143	1428	14,195	1.00	∞
0.025	1.16	86.0	2429	12,767	0.899	0.997
0.035	1.63	61.4	2109	10,338	0.728	0.566
0.045	2.09	47.8	1775	8229	0.580	0.376
0.055	2.56	39.1	1408	6454	0.455	0.263
0.065	3.02	33.1	1051	5046	0.355	0.190
0.075	3.48	28.7	820	3995	0.281	0.144
0.085	3.95	25.3	592	3175	0.224	0.109
0.095	4.42	22.6	443	2583	0.182	8.71×10^{-2}
0.105	4.88	20.5	336	2140	0.151	6.08×10^{-2}
0.115	5.35	18.7	268	1804	0.127	5.88×10^{-2}
0.125	5.81	17.2	208	1536	0.108	5.00×10^{-2}
0.135	6.28	15.9	154	1328	9.35×10^{-2}	4.26×10^{-2}
0.145	6.74	14.8	151	1174	8.27×10^{-2}	3.74×10^{-2}
0.155	7.21	13.9	112	1023	7.21×10^{-2}	3.26×10^{-2}
0.165	7.67	13.0	100	911	6.42×10^{-2}	2.86×10^{-2}
0.175	8.14	12.3	90	811	5.71×10^{-2}	2.53×10^{-2}
0.185	8.60	11.6	71	721	5.08×10^{-2}	2.24×10^{-2}
0.195	9.07	11.0	63	650	4.58×10^{-2}	2.04×10^{-2}
0.205	9.53	10.5	60	587	4.13×10^{-2}	1.83×10^{-2}
0.215	10.0	10.0	47	527	3.71×10^{-2}	1.62×10^{-2}
0.225	10.5	9.55	39	480	3.38×10^{-2}	1.49×10^{-2}
0.235	10.9	9.15	28	441	3.11×10^{-2}	1.37×10^{-2}
0.245	11.4	8.77	34	413	2.91×10^{-2}	1.26×10^{-2}
0.255	11.9	8.43	25	379	2.67×10^{-2}	1.16×10^{-2}
0.265	12.3	8.11	27	354	2.49×10^{-2}	1.08×10^{-2}
0.275	12.8	7.82	22	327	2.30×10^{-2}	1.00×10^{-2}
0.285	13.3	7.54	23	305	2.15×10^{-2}	9.33×10^{-3}

Table 2 (Continued)

Interval Center (in.)	$c \times 10^4$ (in.)	$\frac{1}{c} \times 10^{-2}$ (in.$^{-1}$)	n	Σn	$\frac{\Sigma n}{N}$	$\log\left(1 - \frac{\Sigma n}{N}\right)^{-1}$
0.295	13.7	7.29	21	282	1.99×10^{-2}	8.64×10^{-3}
0.305	14.2	7.05	21	261	1.84×10^{-2}	7.98×10^{-3}
0.315	14.6	6.82	16	240	1.69×10^{-2}	7.33×10^{-3}
0.325	15.1	6.61	21	174	1.22×10^{-2}	5.29×10^{-3}
0.335	15.6	6.42	12	153	1.07×10^{-2}	4.64×10^{-3}
0.345	16.0	6.23	23	133	9.37×10^{-3}	4.07×10^{-3}
0.355	16.5	6.05	15	110	7.75×10^{-3}	3.36×10^{-3}
0.365	17.0	5.89	8	95	6.69×10^{-3}	2.90×10^{-3}
0.375	17.4	5.73	9	86	6.06×10^{-3}	2.63×10^{-3}
0.385	17.9	5.58	10	77	5.42×10^{-3}	2.35×10^{-3}
0.395	18.4	5.44	6	67	4.72×10^{-3}	2.04×10^{-3}
0.405	18.8	5.31	7	61	4.30×10^{-3}	1.87×10^{-3}
0.415	19.3	5.18	8	54	3.80×10^{-3}	1.65×10^{-3}
0.425	19.8	5.06	6	46	3.24×10^{-3}	1.41×10^{-3}
0.435	20.2	4.94	4	40	2.82×10^{-3}	1.23×10^{-3}
0.445	20.7	4.83	4	36	2.53×10^{-3}	1.10×10^{-3}
0.455	21.2	4.72	3	32	2.25×10^{-3}	9.75×10^{-4}
0.465	21.6	4.62	5	29	2.04×10^{-3}	8.85×10^{-4}
0.475	22.1	4.53				
0.485	22.5	4.43	3	24	1.69×10^{-3}	7.33×10^{-4}
0.495	23.0	4.34				
0.505	23.5	4.26	1	21	1.48×10^{-3}	6.41×10^{-4}
0.515	24.0	4.17	2	20	1.41×10^{-3}	6.11×10^{-4}
0.525	24.4	4.09	2	18	1.27×10^{-3}	5.51×10^{-4}
0.535	24.9	4.02				
0.545	25.3	3.94				
0.555	25.8	3.87				
0.565	26.3	3.80	1	16	1.13×10^{-3}	4.90×10^{-4}
0.575	26.7	3.74				
0.585	27.2	3.67	2	15	1.06×10^{-3}	4.60×10^{-4}
0.595	27.6	3.61	2	13	9.16×10^{-4}	3.98×10^{-4}
0.605	28.1	3.55				
0.615	28.6	3.50	1	11	7.75×10^{-4}	3.36×10^{-4}
0.625	29.1	3.44	1	10	7.04×10^{-4}	3.06×10^{-4}
0.635	29.5	3.39				
0.645	30.0	3.33	2	9	6.34×10^{-4}	2.75×10^{-4}
0.655	30.5	3.28	1	7	4.93×10^{-4}	2.14×10^{-4}
0.665	30.9	3.23	1	6	4.23×10^{-4}	1.84×10^{-4}
0.675	31.4	3.18				
0.685	31.9	3.14				
0.695	32.3	3.09				
0.705	32.8	3.05				
0.715	33.2	3.01				
0.725	33.7	2.96	1	5	3.52×10^{-4}	1.53×10^{-4}
0.735	34.2	2.92	1	4	2.82×10^{-4}	1.22×10^{-4}
0.745	34.6	2.89				
0.755	35.1	2.85	1	3	2.11×10^{-4}	9.15×10^{-5}
0.765	35.6	2.81	1	2	1.41×10^{-4}	6.11×10^{-5}
0.775	36.0	2.77				
0.785	36.5	2.74				
0.795	37.0	2.70				
0.845	39.3	2.54	1	1	7.04×10^{-5}	3.05×10^{-5}

The average flaw density in the samples was thus calculated to be 1.04×10^6 flaws per inch^2. This gives a value of 6.92×10^5 flaws per gauge area. Thus, for $G(1/c) = 0.01$, $F(1/c)$ is found by Equation 2 to be 1.59×10^{-8}, and for $G(1/c) = 0.99$, $F(1/c)$ is 6.65×10^{-6}. Therefore, in order to determine a $G(1/c)$ distribution without having to extrapolate $F(1/c)$, experimental values of $F(1/c)$ must be found on the order of 10^{-7}. This means that a total flaw count on the order of 10^8 or 10^9 flaws should be made. To develop a rapid method of measuring the stress-concentrating ability of a flaw with flaw densities in the ranges observed is a problem, since, at a measuring rate of one flaw per second, it would require on the order of 3 to 30 years to record the necessary data.

As the desired experimental values of $F(1/c)$ could not be found, the data which were obtainable in a reasonable amount of time were fitted to a number of exponential distributions. The simplest one, and also one that gave a good fit, was

$$F\left(\frac{1}{c}\right) = 1 - e^{-\alpha(1/c)^{\beta}} , \tag{3}$$

where α and β are parameters determined by plotting log log $[1 - (\Sigma n/N)]^{-1}$ vs log $(1/c)$. A tabulation of $1/c$ and log $[1 - (\Sigma n/N)]^{-1}$ is given in Table 2, and a plot of log log $[1 - (\Sigma n/N)]^{-1}$ vs log $(1/c)$ is shown in Figure 10. For small values of $\Sigma n/N$, the distribution $1 - e^{-\alpha(1/c)^{\beta}}$ with $\alpha = 2.20 \times 10^{-16}$ and $\beta = 4.88$ was found to represent $F(1/c)$ well, and was used to extrapolate values of $1/c$ for the distribution of smallest values, $G(1/c)$, using Equation 3 in Equation 2. The results are shown in Table 3.

Table 3

Extrapolation of c Values for $G(1/c)$ Using Equation 3 in Equation 2.

$G\left(\frac{1}{c}\right)$	$-\ln(1-G)$	$-\frac{1}{n\alpha} \times \ln(1-G)$	$\ln\left(\frac{1}{c}\right)^{\beta}$	$\frac{1}{2.3\beta} \times \ln\left(\frac{1}{c}\right)^{\beta}$	$\frac{1}{c}$	$c \times 10^3$
0.048	0.04919	3.23×10^8	19.59312	1.74144	55.14	18.1
0.095	0.09982	6.56×10^8	20.30163	1.80441	63.69	15.7
0.143	0.15432	1.01×10^9	20.73317	1.84276	69.62	14.4
0.190	0.21072	1.38×10^9	21.04530	1.87051	74.22	13.5
0.238	0.27181	1.78×10^9	21.29983	1.89313	78.19	12.8
0.286	0.33687	2.21×10^9	21.51621	1.91236	81.73	12.2
0.334	0.40647	2.67×10^9	21.70530	1.92917	84.95	11.8
0.381	0.47965	3.15×10^9	21.87062	1.94386	87.87	11.4
0.428	0.55862	3.67×10^9	22.02341	1.95744	90.56	11.0
0.476	0.64626	4.25×10^9	22.16778	1.97027	93.38	10.7
0.523	0.74024	4.86×10^9	22.30426	1.98240	96.03	10.4
0.570	0.84397	5.55×10^9	22.43521	1.99404	98.64	10.1
0.618	0.96233	6.32×10^9	22.56694	2.00575	101.3	9.87
0.666	1.09362	7.18×10^9	22.69450	2.01709	104.0	9.61
0.714	1.25176	8.22×10^9	22.83101	2.02922	107.0	9.34
0.716	1.43129	9.40×10^9	22.96499	2.04113	109.9	9.10
0.810	1.66073	1.09×10^{10}	23.11198	2.05488	113.5	8.81
0.850	1.89712	1.25×10^{10}	23.24092	2.06565	116.3	8.60
0.900	2.30259	1.51×10^{10}	23.43791	2.08316	122.1	8.19
0.952	3.63655	1.99×10^{10}	23.71394	2.10769	128.1	7.81

Average number of flaws per gauge area = 6.92×10^5

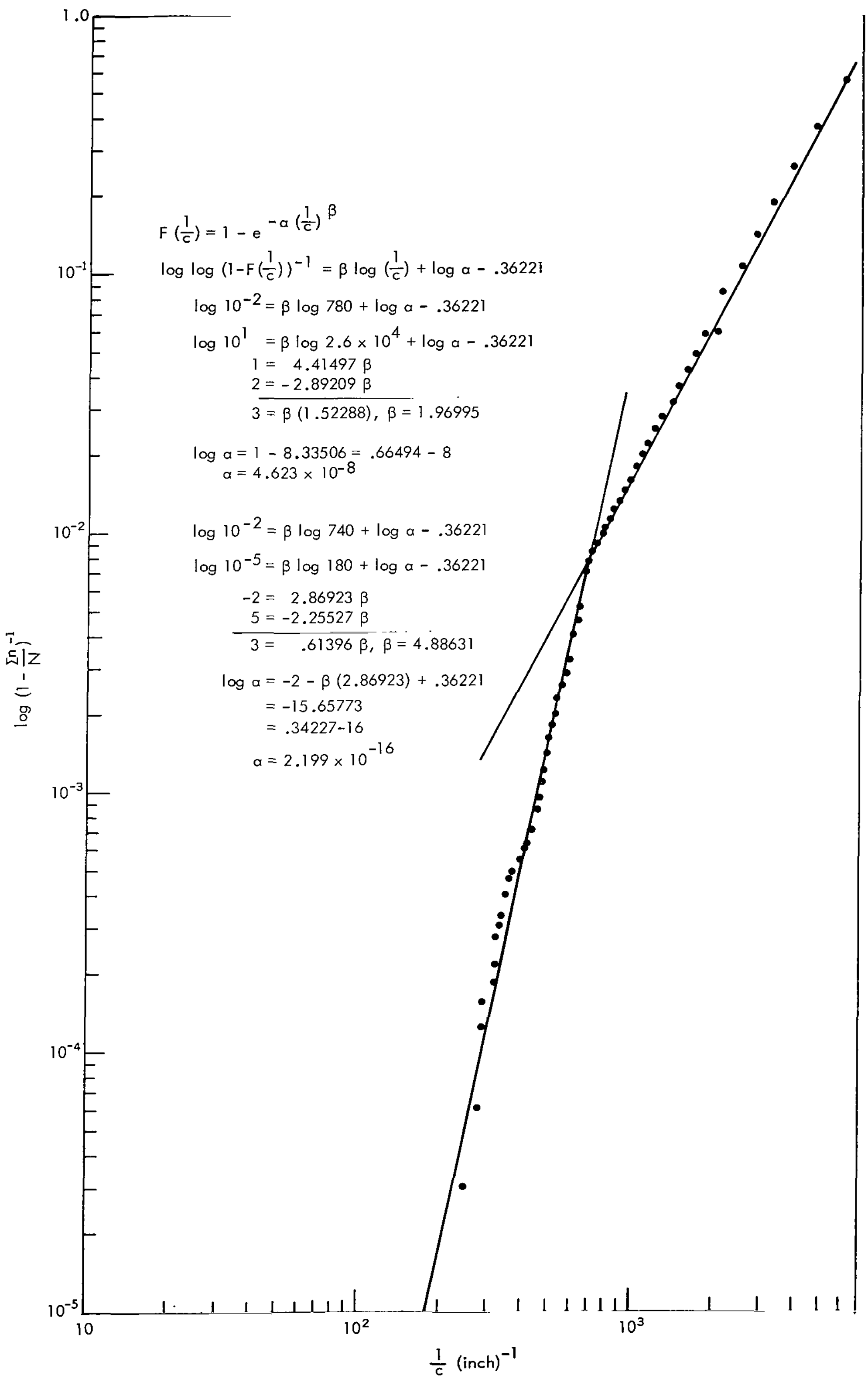

Figure 10—Plot of log (1/c) vs log log $(1-\Sigma n/N)^{-1}$.

The samples were failed and, using Equation 1, the fracture probability, $S(\sigma)$, was computed. A functional relation between σ and $1/c$ of the form $\sigma = M(1/c)^p$ was assumed, and for equal values of $S(\sigma)$ and $G(1/c)$ the value of $\log(\sigma)$ was plotted vs $\log(1/c)$. The result is shown in Figure 11. A tabulation of $\log(\sigma)$ and $\log(1/c)$ for equal values of $S(\sigma)$ and $G(1/c)$ is given in Table 4.

Gauge-size pieces of failed specimens were scanned with a microscope, and the maximum linear dimension of the largest pore or grain pullout was recorded. These values are given in Table 1.

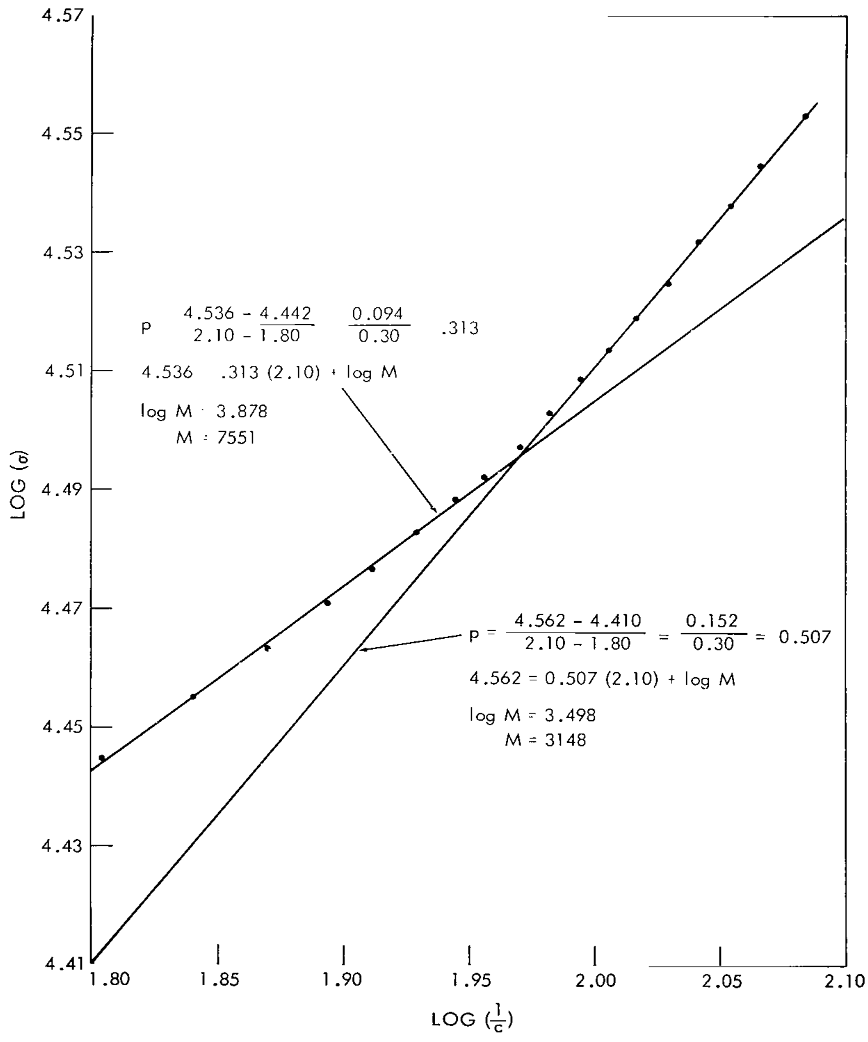

Figure 11—Plot of log σ vs log(1/c) for equal values of $S(\sigma)$ and $G(1/c)$.

Table 4

Tabulation of $\log(\sigma)$ and $\log(1/c)$ for Equal Values of $S(\sigma)$ and $G(1/c)$.

$S(\sigma)$ or $G(1/c)$	$\sigma \times 10^{-3}$	$\log(\sigma)$	$1/c$	$\log(1/c)$
0.048	26.959	4.43249	55.14	1.74144
0.095	27.807	4.44514	63.69	1.80441
0.143	27.952	4.45576	69.62	1.84276
0.190	29.022	4.46389	74.22	1.87051
0.238	29.563	4.47070	78.19	1.89313
0.286	29.720	4.47712	81.73	1.91236
0.334	30.012	4.48287	84.95	1.92917
0.381	30.452	4.48855	87.87	1.94386
0.428	31.078	4.49248	90.56	1.95744
0.476	31.168	4.49776	93.38	1.97027
0.523	31.315	4.50365	96.03	1.98240
0.570	31.908	4.50840	98.64	1.99404
0.618	32.937	4.51388	101.3	2.00575
0.666	34.675	4.51943	104.0	2.01709
0.714	34.721	4.52530	107.0	2.02922
0.761	34.846	4.53212	109.9	2.04113
0.810	34.914	4.53857	113.5	2.05488
0.850	34.948	4.54507	116.3	2.06565
0.900	36.181	4.55328	122.1	2.08316
0.952	36.314	4.56086	128.1	2.10769

Assume $\sigma = M(1/c)^p$.

Then $\log \sigma = p \log(1/c) + \log M$.

RESULTS AND DISCUSSION

The Griffith equation for fracture strength (Reference 7) is

$$\sigma = \sqrt{\frac{\pi E \gamma}{c\left(1 - \nu^2\right)}} ,$$

where

E = modulus of elasticity,

γ = specific surface energy of new surfaces formed,

c = major diameter of an elliptical crack, and

ν = Poisson's ratio.

Values of E and ν are given (Reference 8) as 52×10^6 psi and 0.21, respectively. The surface energy, γ, associated with the fracture process generally consists of a number of components among which is the chemical surface free energy. Recent values of γ reported for single crystalline material range from 6.0 to 7.3 J/m^2 depending on crystal orientation (Reference 9). Using an average value of 6.6 J/m^2 or 3.76×10^{-2} in.-lbs/in.^{2}, one gets $\sigma = 2.54 \times 10^3\ (1/c)^{1/2}$ for c expressed in inches and σ expressed in pounds per square inch.

A rough estimate of the applicability of an equation of the Griffith form using this analysis is offered in Figure 11. As shown, the data depict more of a curve than a straight line; however, the curve is well defined by two lines. The upper line has a slope and an intercept which are in order with those of the Griffith equation.

If the strength of a material is governed by a surface flaw distribution, and if one considers only the uniformly stressed central portion of a beam under four-point loading, then the Weibull equation for probability of fracture (Reference 10) is

$$S = 1 - e^{-A(\sigma-\sigma_\mu/\sigma_0)^m},$$

where

A = the gauge area of samples tested,

σ = the actual fracture stress,

σ_μ = the stress below which fracture cannot occur,

σ_0 = a material constant, and

m = a constant representative of the flaw density.

The Weibull equation with $\sigma_\mu = 0$ and Equation 3 are quite similar if σ is substituted for $1/c$ using an equation of the Griffith form. The result is

$$F(\sigma) = 1 - e^{-A'\sigma^{m'}},$$

where $A' = \alpha/M^{\beta/p}$ and $m' = \beta/p$.

The shape of the curve in Figure 10 is interesting because of the kink in it. This suggests a bimodal distribution of flaws. Pores and grain pullouts are visually indistinguishable in most cases, and no attempt at distinguishing between them was made while counting flaws for this analysis. It is therefore possible that this kink is the result of superposing the two flaw distributions.

CONCLUSIONS

A thorough characterization of 20 high-alumina (99.5 percent Al_2O_3) flexure specimens established the presence of the following types of flaws:

grain pullouts due to polishing

polishing scratches
pores
grain boundaries
dislocations in individual grains.

Application of a statistical correlation procedure which relates strength to flaw "magnitude" demonstrated the need for considerable extrapolation. The fact that there is order-of-magnitude agreement between observed and calculated values of $c(max)$ indicates an internal consistency, and therefore the assumptions made were reasonably accurate. Considering the clarity with which $S(\sigma)$ was defined using only 20 specimens, the fact that a plot of $\log(\sigma)$ vs $\log(1/c)$ for equal values of $S(\sigma)$ and $G(1/c)$ is a continuous curve and compares with the Griffith equation indicates that a more exhaustive investigation which systematically attacks some problems brought out by this investigation may prove fruitful (at least in the area of material predictability).

This investigation has established the following problems:

1. Determining what type of flaw (if indeed there is just one type) nucleates fracture in a brittle polycrystalline material, such as a sintered Al_2O_3 compact, is a problem. Undoubtedly there is interaction between flaw networks, and such interaction could preclude separation of the networks and prevent superposing their effects.

2. Determining a measurement or series of measurements which significantly characterizes the stress-concentrating ability of existing flaws is a problem.

3. Devising a counting device which measures the "magnitude" of a flaw and does it at such a rate as to make practical an experimental determination of parent flaw distributions is a problem.

Solution of the last of these problems is necessary to the confident application of a statistical correlation procedure based on the "weakest-link" concept. Actually, if a parent flaw population could be adequately characterized experimentally, such a procedure could be used to pragmatically test possible solutions to the first two problems. This, of course, assumes applicability of a weakest-link type theory in which, conceptually at least, one is dealing with the breakage of a chain with links joined in series with the force on each link equal to the force applied to the chain as a whole.

Goddard Space Flight Center
National Aeronautics and Space Administration
Greenbelt, Maryland, December 1, 1969
601-13-02-42-51

REFERENCES

1. Lynch, J. F., Ruderer, C. G., and Duckworth, W. H., "Engineering Properties of Selected Ceramic Materials" (Appendix 7.1), Columbus, Ohio: The American Ceramic Society, Inc., 1966.

2. Pears, D. C., Oglesby, S., Davidson, J. I., Gillis, G. F., Digesu, F. J., and Carlson, C. L., "Evaluation of Tensile Data for Brittle Materials Obtained with Gas Bearing Concentricity," Technical Documentary Report No. ASD-TDR-63-245, Air Force Systems Command, Wright-Patterson Air Force Base, Ohio, May 1963.

3. Epstein, Benjamin, "Statistical Aspects of Fracture Problems," *Journal of Applied Physics* 19, 140-147, February 1948.

4. Parikh, N. M., "Studies of the Brittle Behavior of Ceramic Materials," Technical Documentary Report No. ASD-TR-61-628, Part III, Air Force Systems Command, Wright-Patterson Air Force Base, Ohio, June 1964.

5. Mar, Henry Y. B., "Fracture Induced in Bicrystals of Aluminum Oxide by Anisotropic Thermal Expansion," Ph.D. thesis, University of Washington, 1968.

6. Ku, R. C., and Johnston, T. L., "Fracture Strength of MgO Bicrystals," *Philosophical Magazine* 9, 231-247, February 1964.

7. Sneddon, I. N., "The Distribution of Stress in the Neighbourhood of a Crack in an Elastic Solid," *Proc. Roy. Soc.* (London) A187: 229-260, 22 October 1946.

8. Coors Bulletin No. 952, "Mechanical, Thermal and Electrical Properties of Coors Alumina and Beryllia Ceramics," Coors Porcelain Company, Golden, Colo., p. 6.

9. Wiederhorn, S. M., "Fracture of Sapphire," Institute of Materials Research, NBS, Washington, D. C. 20234.

10. Weil, N. A., and Daniel, I. M., "Analysis of Fracture Probabilities in Nonuniformly Stressed Brittle Materials," *Jour. Am. Cer. Soc.* 47(6):268-274, 1964.

NASA-Langley, 1970 —— 18

"The aeronautical and space activities of the United States shall be conducted so as to contribute . . . to the expansion of human knowledge of phenomena in the atmosphere and space. The Administration shall provide for the widest practicable and appropriate dissemination of information concerning its activities and the results thereof."

—NATIONAL AERONAUTICS AND SPACE ACT OF 1958

NASA SCIENTIFIC AND TECHNICAL PUBLICATIONS

TECHNICAL REPORTS: Scientific and technical information considered important, complete, and a lasting contribution to existing knowledge.

TECHNICAL NOTES: Information less broad in scope but nevertheless of importance as a contribution to existing knowledge.

TECHNICAL MEMORANDUMS: Information receiving limited distribution because of preliminary data, security classification, or other reasons.

CONTRACTOR REPORTS: Scientific and technical information generated under a NASA contract or grant and considered an important contribution to existing knowledge.

TECHNICAL TRANSLATIONS: Information published in a foreign language considered to merit NASA distribution in English.

SPECIAL PUBLICATIONS: Information derived from or of value to NASA activities. Publications include conference proceedings, monographs, data compilations, handbooks, sourcebooks, and special bibliographies.

TECHNOLOGY UTILIZATION PUBLICATIONS: Information on technology used by NASA that may be of particular interest in commercial and other non-aerospace applications. Publications include Tech Briefs, Technology Utilization Reports and Notes, and Technology Surveys.

Details on the availability of these publications may be obtained from:

SCIENTIFIC AND TECHNICAL INFORMATION DIVISION

NATIONAL AERONAUTICS AND SPACE ADMINISTRATION

Washington, D.C. 20546